

# A HYBRID METHOD FOR MEASURING HEAT FLUX

David O. Hubble and Tom E. Diller.  
*Virginia Polytechnic Institute and State University*

**This paper reports on the development and evaluation of a novel hybrid method for obtaining heat flux measurements. By combining spatial and temporal temperature measurements, it is shown that both the time response and accuracy of a heat flux sensor can be improved. This hybrid method was shown to increase the time response of a heat flux sensor mounted on a high conductivity material by a factor of 28 compared to a standard spatial sensor. Furthermore, this analysis allows the heat flux sensor to be much less sensitive to the material to which it is mounted. It was shown that changing the thermal conductivity of the backing material four orders of magnitude caused only an 11% change in sensor error. This method is validated both numerically and experimentally and demonstrates significant improvement compared to operating the sensor as a spatial or temporal sensor alone.**

## 1. Introduction

Modeling of thermal systems requires a combination of temperatures and energy fluxes for prediction of their performance. Temperatures are commonly measured by a variety of standard methods, but the measurement of heat flux is a particular challenge because it is an energy flux normal to a plane of material rather than a property of a material. Therefore, sensors to measure heat flux usually must be mounted onto a material that provides a good heat sink so that the energy flow is not impeded. This makes it very difficult to use heat flux gages to measure heat flux on materials that are not good thermal conductors. The purpose of this paper is to present a new method which allows heat flux gages to make accurate measurements on any type of backing material. Applications include furnaces to thermal protection systems for spacecraft.

## 2. Background

Two of the most common modes of heat flux measurement are that of a differential heat flux sensor and that of a slug calorimeter [1]. A differential heat flux sensor measures the temperature difference over a spatial distance with a known thermal resistance, as illustrated in Fig. 1. This gives the heat flux through the sensor from the steady-state version of Fourier's Law with  $k$  as the thermal conductivity of the resistance layer and  $\delta$  as the thickness of the resistance layer.  $T_1$  is

the temperature of the exposed face while  $T_2$  is the temperature at the back of the sensor.

$$q''_{\text{Differential}} = k \frac{T_1 - T_2}{\delta} \quad (1)$$

Under steady-state conditions the heat flux entering the sensor in Fig. 1,  $q_1''$ , is equal to that leaving,  $q_2''$ . Hager [2] calculated the 98% response time to a step change of heat flux at the surface in terms of the sensor's thickness and thermal diffusivity. This is often considered as steady-state.

$$t_{ss} = 1.5 \frac{\delta^2}{\alpha} \quad (2)$$

Hager's [2] analysis was performed on the ideal case of a sensor mounted on a perfect heat sink where the backside temperature,  $T_2$ , remains constant.

In a slug calorimeter the amount of thermal energy absorbed by the sensor is measured as a function of time. The rate of change of the sensor's temperature is measured and its thermal capacitance is known. Conservation of energy for a control volume surrounding the sensor "slug" yields

$$q''_{\text{Slug}} = \rho C \delta \frac{dT_{ave}}{dt} = q_1'' - q_2'' \quad (3)$$

where  $\rho C \delta$  is the thermal mass of the slug per sensor area.

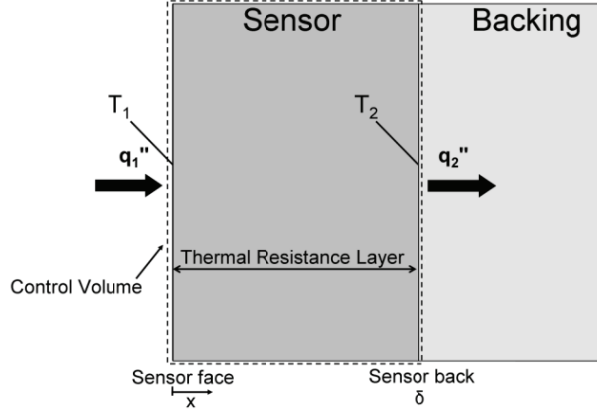


**Fig. 1 Sensor-backing system**

The heat loss ( $q_2''$ ) is normally minimized by insulating all but the front surface. If the average temperature within the slug were known, Eq. (3) would perfectly measure the net heat flux into the slug. However, since it is not possible to measure the average temperature, the slug is typically made from a high conductivity material and the temperature at the back surface approximates the slug's average temperature. Therefore, for a short time after a heat flux is applied to the slug, thermal energy is being absorbed by the slug (the slug's average temperature is increasing) before any heat has reached the back surface. This causes a delay before the slug accurately measures the actual net heat flux. The 99% response time to a step change of heat flux at the surface is given as

$$t_{ss} = 0.54 \frac{\delta^2}{\alpha} \quad (4)$$

by Hightower [3]. This analysis was performed assuming a perfectly insulated backside surface ( $q_2''=0$ ).

While these two modes of operation can be adequately used for specific measurement applications, they both have serious limitations. For example, for a differential gage to have a fast time response, it must be very thin. This is difficult to achieve in harsh environments where sensors typically must be made with a substantial thickness to survive. Also, since a differential sensor only measures heat flowing through it, it must be provided with a good heat sink. This necessitates its mounting on or in a high conductivity material, not an insulator. The main problems encountered when using a slug calorimeter include adequately insulating the slug to minimize losses as well as designing the slug to be as unobtrusive as possible. Also, since the output of a slug is proportional to the rate at which its temperature is changing, it is unable to measure a heat flux at steady-state. It is worth

noting that the design criteria for these two types of sensors are opposite. A differential gage more accurately measures  $q_1''$  when  $q_2''$  is maximized with minimal heat storage in the gage. Conversely, a slug calorimeter needs to minimize  $q_2''$  and maximize the stored thermal energy.

A number of papers have reported using a combination of the spatial and temporal changes of temperature to infer or improve heat flux measurements. Kidd and Adams [4] used finite-element analysis to determine a response function for their Schmidt-Boelter heat flux gages. This was used to compensate for the energy deficit caused by the thermal capacitance of this differential style gage. They were able to substantially increase the time response of the heat flux measurements for their transient tests in high speed wind tunnels. A complete analysis of a simpler thin polyimide differential gage was performed by Guenette and Epstein [5]. This enabled measurements from steady-state to 100 kHz on metal turbine blades, but required solution of the equations for one-dimensional transient conduction. A "plug-type heat flux gauge" was developed by Liebert [6] to account for the combination of conduction and storage in the post normal to the surface. Four temperatures were measured along the post as a function of time and compared with transient temperature solutions to determine the surface heat flux. Experimental results were obtained for metal turbine blade models. Unfortunately, the method did not work well when the sensor was mounted in a low thermal conductivity material [7].

Clearly, there are advantages to including both the differential and slug type responses for measuring heat flux. It would be beneficial to design a simple sensor and analysis scheme which could utilize the advantages of these two sensor types together while minimizing their negative characteristics. It is with this goal in mind that the following analysis was done for such a hybrid heat flux (HHF) design with a simple one-dimensional sensor.

### 3. HHF Methodology

**3.1 Differential Term.** Fig. 1 shows the schematic of a one-dimensional heat flux sensor. The quantity  $q_1''$  represents the heat flux into the sensor face, which is the desired measurement. Fig. 2 depicts a typical temperature profile that would result from a heat flux, applied at the left surface, which diffuses through the sensor and into the backing material. These profiles will be non-linear until the entire system reaches steady-state at which point both curves will become linear. From Fourier's law,

$$q'' = -k \frac{dT}{dx} \quad (5)$$

the heat conduction at any point can be calculated from the slope of this temperature profile as long as the thermal conductivity is known.

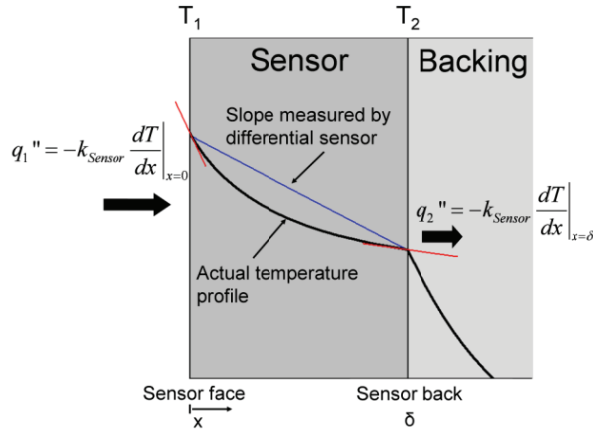


**Fig. 2 Temperature profile with sensor-backing system**

A differential heat flux sensor measures the temperature at the front and back surfaces of the sensor and indicates the heat flux based on the thickness and the thermal conductivity. Fig. 2 shows, however, that when the sensor is not at steady-state, the slope (and therefore the heat flux) that the differential sensor is measuring (Eq. (1)) is different from that at the sensor face. Whenever the sensor is in a quasi-steady state, however, the slope measured by the differential sensor is almost exactly the average of the slopes at the two surfaces. For example, it can be shown that this is exactly true for any quadratic temperature profile,  $T(x) = ax^2 + bx + c$ ,

$$\underbrace{\frac{1}{2} \left( \left. \frac{dT}{dx} \right|_{x=x_1} + \left. \frac{dT}{dx} \right|_{x=x_1+\delta} \right)}_{\text{Average of two slopes}} = \underbrace{\frac{T(x_1 + \delta) - T(x_1)}{\delta}}_{\text{Slope measured by differential sensor}} \quad (6)$$

$$2ax_1 + a\delta + b$$

The time required for the slope measured by the differential sensor to equal the average of the slopes at the two surfaces to within 2% was determined

numerically using the transient conduction code described in section IV. Converted to the non-dimensional Fourier number ( $Fo = at/\delta^2$ ), this time was 0.51 for a perfectly insulated backing and 1.15 for a perfectly conducting backing. For a typical ceramic gage [8] with a thickness of 500 $\mu$ m and thermal diffusivity of 1.0E-6 m<sup>2</sup>/s, this corresponds to a time of 30.3 milliseconds on a perfect conductor. A metal gage [9] with a thickness of 3.2mm and thermal diffusivity of 5.5E-6 m<sup>2</sup>/s gives a time of 2.12 seconds on a perfect conductor. The required times on insulators will be quicker since the Fourier number was smaller (0.51 vs. 1.15) for that scenario.

Under these quasi-steady conditions, Eq. (6) can be used to relate the heat fluxes  $q_1''$  and  $q_2''$ . The temperature slopes at the sensor front and back surfaces represent the heat flux into and out of the sensor, respectively, and the differential sensor heat flux is proportional to the total temperature difference,  $T_1 - T_2$ . Substituting the corresponding heat fluxes into Eq. (6) gives

$$\frac{q_1'' + q_2''}{2} = q_{\text{Differential}}'' = k \frac{T_1 - T_2}{\delta} \quad (7)$$

**3.2 Slug Term.** A slug calorimeter measures heat flux by measuring the rate at which heat is absorbed by the slug. The absorbed flux represents the net heat flux into the control volume,  $q_1'' - q_2''$ , as shown in Fig. 2. Eq. (3) stated that this net heat flux can be measured using a slug calorimeter which measures the time rate of change of the slug's average temperature. As mentioned, the standard method for measuring this average temperature is to measure the temperature at the back of the sensor and assume that this approximates the actual average temperature. This is a valid assumption once enough time has passed for the heat that enters the sensor face to reach the sensor back. However, for the sensor shown in Fig. 1, both surface temperatures are known. By utilizing the temperature measurement at the sensor surface, a more accurate measure of the absorbed heat flux can be made. Subsequently, the sensor can be operated as a slug calorimeter in three different modes; the sensor's temperature can be approximated by the front temperature, the back temperature, or an average of the two. The response of a slug calorimeter to a step change in heat flux while mounted on a perfect insulator using these three methods is shown in Fig. 3.

As shown in Fig. 3, utilizing only the surface temperature offers no advantages compared to only using the back temperature as it takes just as long for an accurate measurement to be made. On the other hand, utilizing the average of both temperatures has advantages and drawbacks. By utilizing both the top and bottom temperatures, the time response increases by more than a factor of three compared to using only

$T_2$  but this temporal increase is accompanied by a large overshoot.

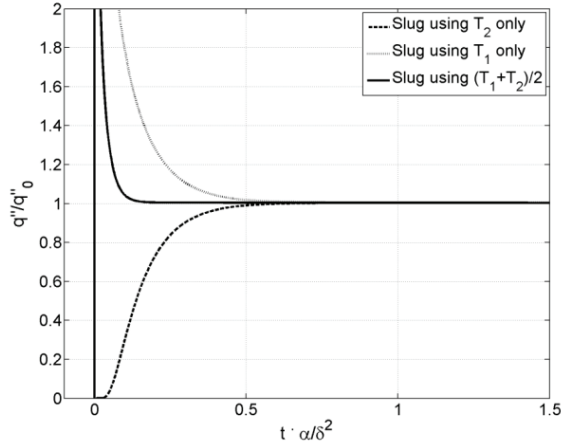


**Fig. 3 Comparison of slug calorimeter response using different temperature measurements**

The overshoot associated with using  $T_1$  in the slug measurement is a result of the  $\sqrt{t}$  dependence of the surface temperature which has an infinite derivative at  $t=0$ . While the overshoot associated with using the average of the two surface temperatures is initially large, its error is smaller than the standard method for all Fourier numbers greater than 0.02. Therefore, in many situations it is advantageous to utilize this average temperature in order to increase the temporal response of the sensor. From this point on,  $q''_{\text{slug}}$  will denote a slug calorimeter that utilizes the average of  $T_1$  and  $T_2$  unless specified otherwise.

$$q''_{\text{slug}} = \rho C \delta \frac{d}{dt} \left( \frac{T_1 + T_2}{2} \right) = q_1'' - q_2'' \quad (8)$$

**3.3 Hybrid Heat Flux.** To combine the spatial and temporal responses of a heat flux sensor, only Eqs. (7) and (8) are needed, as repeated here.

$$q_1'' + q_2'' = 2q''_{\text{Differential}} \quad (9)$$

$$q_1'' - q_2'' = q''_{\text{Slug}} \quad (10)$$

Combining Eqs. (9) and (10), and solving for the desired  $q_1''$  yields

$$q_1'' = q''_{\text{Differential}} + \frac{1}{2} q''_{\text{Slug}} \quad (11)$$

Equation (11) shows how the outputs of a differential sensor and a slug calorimeter can be combined. This hybrid of the spatial and temporal responses can be used to more accurately measure the heat flux at the sensor surface,  $q_1''$ . While this represents a simple model, it was derived from basic thermal energy conservation.

The validity of Eq. (11) can be supported by examining two limiting cases. First, consider the limit of a perfectly insulating backing material. For this case, the one-dimensional heat equation within the sensor simplifies to

$$\frac{d^2 T}{dx^2} = \text{Const.} \quad (12)$$

once quasi-steady state is reached. The solution to this equation yields a temperature profile within the sensor that will be perfectly quadratic with a slope of zero at  $x=\delta$  since  $q_2''=0$ . This means, using Eq. (6), that the differential sensor will measure exactly half the heat flux entering the sensor. That is,  $q''_{\text{Differential}} = \frac{1}{2} (q_1'' + q_2'') = \frac{1}{2} (q_1'' + 0) = \frac{1}{2} q_1''$ . Also, since  $q_2''$  is exactly zero for this case, the slug calorimeter will measure the heat flux perfectly, i.e.  $q''_{\text{slug}} = q_1''$ . Therefore, the hybrid method described in Eq. (11) will exactly measure the correct heat flux for this case.

Another limiting case occurs when the entire system is at steady-state on a perfect heat sink ( $d^2 T/dx^2=0$ ). For this case, the temperature profile within the sensor is linear. Consequently, the differential sensor will measure the exact heat flux;  $q''_{\text{Differential}} = q_1''$ . Also, since the system is at steady-state, the time derivative of the temperature everywhere in the sensor is zero and the slug calorimeter will measure zero heat flux. Once again, the HHF method (Eq. (11)) perfectly handles this limiting case.

The HHF method requires that a sensor be designed such that  $T_1$ ,  $T_2$ , and  $\Delta T$  are measured. However, accurately measuring any two of these allows the third to be calculated since  $\Delta T = T_1 - T_2$ . For the two sensors already mentioned [8, 9] this will not require any change in design as these sensors already measure the required temperatures. Also, none of the aforementioned analysis placed any requirements on which temperatures were used in evaluating the slug calorimeter term. That is, Eq. (8) is valid regardless of which temperatures are used. As will be seen, changing which temperatures are used to evaluate this term will significantly affect the performance of the HHF method.

#### 4. HHF Numerical Validation

In order to validate the HHF concept, 1-D transient conduction through the sensor-backing system (Fig. 1) was modeled using finite-difference computations. This was done using an in-house developed code which utilizes an implicit discretization of the 1-D heat equation in MATLAB. The derivation of this discretization can be found in [10]. The boundary conditions at the sensor face allowed any thermal condition to be applied including time varying fluxes and convective or radiative conditions. Temporal and

spatial steps were kept sufficiently small to eliminate any grid and time step dependence. This was verified for the parameters shown in Table 1 by increasing both the temporal and spatial resolution by a factor of ten and comparing the results to those obtained using the lower resolution. In both cases, the discrepancy was less than 0.1%. Changing material properties as well as the thickness of the sensor allowed for any sensor design to be tested. Also, the material properties and thickness of the backing material could be varied to investigate how this affected sensor performance. For all numerical simulations shown, the high temperature heat flux sensor (HTHFS) [9] was modeled mounted on a backing material three times thicker than the sensor. It was verified that the backing material thickness did not significantly affect the analysis. This was done by varying the thickness from one to ten times the thickness of the sensor which caused less than a 3% change in sensor performance. For all tests, the boundary condition at the back surface of the backing material was held at a constant temperature. Table 1 summarizes the parameters used in the numerical simulations.

**Table 1 Parameters used in numerical simulation**

Parameter	Value	Units
Sensor thermal conductivity	22	W/m K
Sensor density	7278	kg/m <sup>3</sup>
Sensor specific heat	548	J/kg K
Sensor thickness	3.175	mm
Backing thickness	9.525	mm
Backing thermal conductivity	0.22 to 2200	W/m K
Spatial step	0.03175	mm
Time step	0.5	ms

At each time step in the code, the temperatures at the face and back of the sensor ( $T_1$  and  $T_2$ ) were recorded. This allowed the sensor's performance in all three modes of operation to be evaluated using only these two temperature histories along with the sensor's properties. The sensor's response to a step heat flux of  $q_0''$  is plotted against Fourier number (dimensionless time) in Fig. 4.

The properties of the backing material were identical to the properties of the sensor. As a slug calorimeter, the sensor's accuracy falls off with time while the differential sensor's accuracy increases with time. This is due to the fact that as the temperature of the sensor increases, more and more heat is conducted through the sensor into the backing material ( $q_2''$  is increasing). Figure 4c shows the speed and accuracy of the HHF method. Not only does the HHF capture the transient better than the slug calorimeter, it settles to the

steady state value much more quickly than the differential sensor.

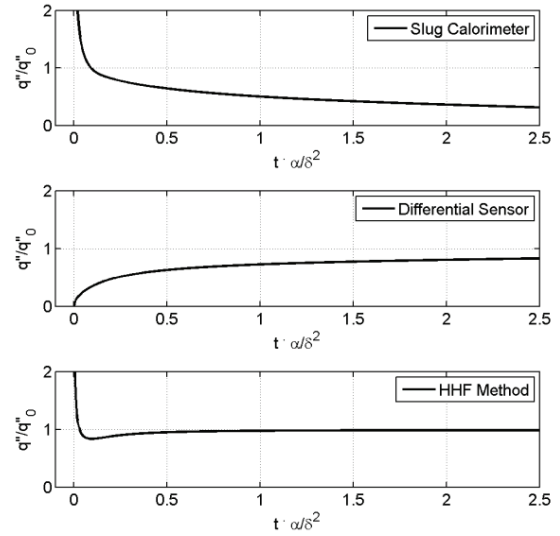
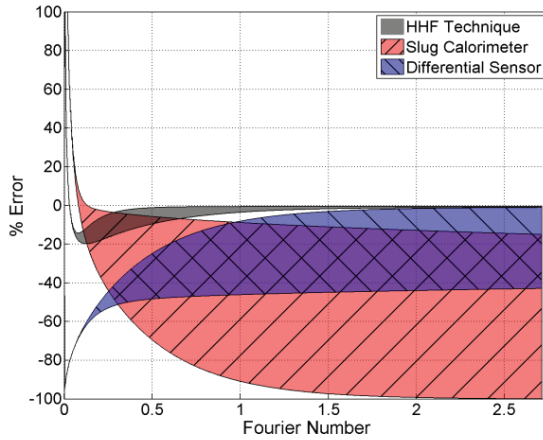


**Fig. 4 Simulated response of sensor in three modes of operation**

While Fig. 4 showed the response of the three methods to a step input while mounted on a material with the same properties as the sensor, this analysis can be extended. Fig. 5 shows the error of the three methods as a function of time and backing material thermal conductivity. In these tests, the backing material's thermal conductivity was stepped from 100 times lower than that of the sensor to 100 times greater. Then, for each backing material, the analysis was run and the error to a step change in  $q_1''$  was calculated as a function of time. These errors define specific regions as shown and demonstrate the potential of the HHF. Not only is the HHF more accurate and faster than both the differential sensor and the slug calorimeter, its performance is also much less dependent on the properties of the backing material as indicated by the much narrower region. In fact, although the backing material thermal conductivity is varied by four orders of magnitude, at no point does this cause more than an 11% change

This analysis also allows the response time to be calculated as a function of backing material properties. The HHF method obtains accuracy to within 2% at a Fourier number of 0.33 when mounted on an insulator and 1.40 when mounted on a conductor. Even on a perfect conductor, which is the best case scenario for a differential sensor, the HHF is faster ( $Fo=1.4$  vs. 1.5). Finally, it is worth noting that for all Fourier numbers greater than 0.02, the error of the HHF is never more than  $\pm 20\%$  regardless of backing material. For

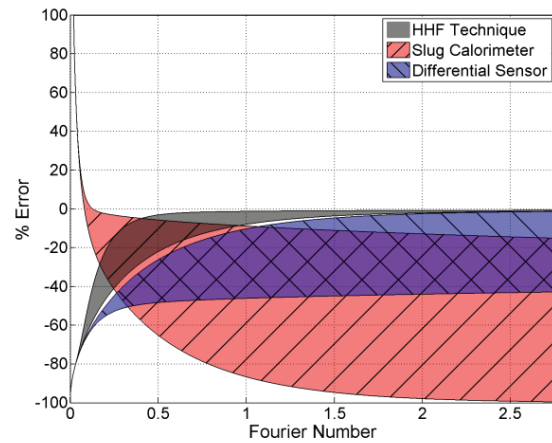
comparison, a differential sensor requires a Fourier number greater than 0.57 to measure the heat flux to within  $\pm 20\%$  on a perfect conductor, 28 times slower than the HHF. in the error of the HHF.



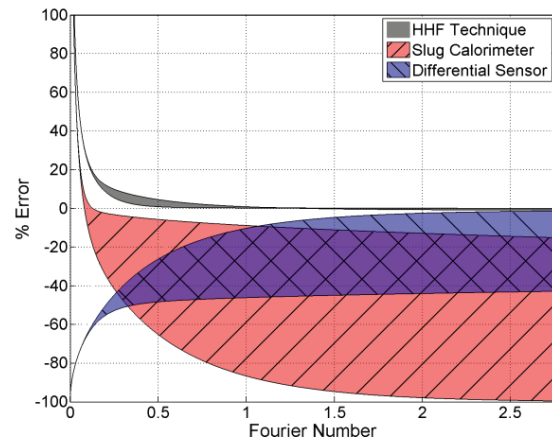
**Fig. 5 Error as a function of time and backing material thermal conductivity**

Fig. 4 and Fig. 5 demonstrate the response of the HHF method to a step change in heat flux while mounted on a wide range of backing material thermal conductivities. The primary limitation with the HHF method is the large overshoot in heat flux at Fourier numbers less than 0.02. As discussed previously, this is due to using the surface temperature in the slug calorimeter term (Eq. (8)). In certain situations, it would be desirable to eliminate this overshoot. This can be accomplished by using only the back temperature ( $T_2$ ) in the slug calorimeter term which eliminates the overshoot at the cost of a slower time response as shown in Fig. 3. The effect that this change has on a sensor using the hybrid method is shown in Fig. 6. Hereafter, if the slug term of the hybrid method only includes the back temperature ( $T_2$ ), it will be referred to as the HHF<sub>2</sub> method. Fig. 6 shows that there is no overshoot and the HHF<sub>2</sub> method still accurately measures the steady-state heat flux regardless of backing material. The only drawback to this method is its slower response time compared to the standard HHF method. While the time required to reach an accuracy of 2% is essentially unchanged, the time required for accuracy within 20% is drastically different. As previously mentioned, for any Fourier number greater than 0.02 the HHF was within 20%. With the HHF<sub>2</sub> method a Fourier number greater than 0.57 is required, the same as for a differential sensor on a perfect conductor. This implies that if the sensor is perfectly heat sunk, the HHF<sub>2</sub> method offers no advantages compared to a standard differential sensor.

For all real materials, however, the HHF<sub>2</sub> method is superior to either the differential sensor or the slug calorimeter. At the other extreme, the hybrid method was applied with the slug term only containing  $T_1$  (HHF<sub>1</sub>). This response is shown in Fig. 7 and demonstrates the versatility of the hybrid method. By simply changing the weighting of  $T_1$  and  $T_2$  in the slug term the response can be changed drastically. Fig. 5 through Fig. 7 show that as the ratio  $T_1/T_2$  in the slug term of the hybrid method increases, the overshoot increases and the response time decreases. In this case, accuracy within 2% is obtained at a Fourier number of 0.75 which represents a significant improvement compared to the value of 1.40 for the standard hybrid method shown in Fig. 5.



**Fig. 6 Error of HHF<sub>2</sub> using only  $T_2$  in slug calorimeter term of HHF compared to standard methods**



**Fig. 7 Error of HHF<sub>1</sub> using only  $T_1$  in slug calorimeter term of HHF compared to standard methods**

On the other hand, accuracy within 20% doesn't occur until a Fourier number of 0.125 is reached instead

of 0.02 which is significantly slower. With this in mind, it is worth noting that Fig. 6 and Fig. 7 represent two extremes for implementing the hybrid method and which method is best must be determined on a case by case basis. If no overshoot can be tolerated,  $T_2$  should be heavily weighted. On the other hand, if response time is critical and some overshoot can be tolerated,  $T_1$  should be more heavily weighted. Some experimentation might be required to determine the optimal weighting for a given set of measurements. The case where the two temperatures are weighted evenly (Fig. 5) is shown as a good tradeoff between overshoot and response time.

### 5. HHF Experimental Validation

To further validate the hybrid method, it was applied to a sensor which was tested experimentally. The sensor tested was the HTHFS [9] which measures a top and bottom surface temperature as well as the differential temperature of a thermal resistance layer. This sensor was tested using two backing conditions; water cooled and insulated. The testing was performed in a stagnating jet convection stand which was fully characterized by Gifford et al. [11]. This stand, shown in Fig. 8, consists of a fully adjustable T-nozzle which directs a jet of hot air at both

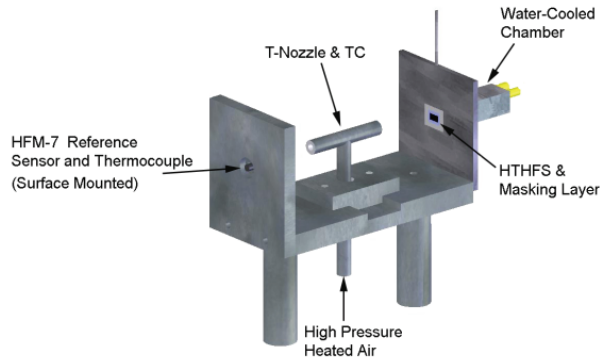


**Fig. 8 Stagnation flow convection calibration facility**

the test sensor and a Vatel Corp. HFM-7® reference sensor. This sensor measures both heat flux and surface temperature and has been shown to have a time response better than 100 kHz [12]. The turbulent heat transfer coefficient on each side of the T-nozzle is identical to within approximately 3% at the stagnation point. The jet recovery temperature ( $T_r$ ) was measured by stretching thin type K thermocouples in the flow 1mm above the two sensors. These two recovery temperatures were identical to within 4%. Using the HFM's heat flux and surface temperature output with the measured jet recovery temperature, the convective heat transfer coefficient was calculated.

$$h = \frac{q''_{HFM}}{T_r - T_{S_{HFM}}} \quad (13)$$

The heat transfer coefficient is shown as a function of time in Fig. 9. This coefficient is constant on the mean to within 2% throughout the test. Once the convective heat transfer coefficient is known, the heat flux to the test sensor can be calculated using the recovery temperature and the measured surface temperature of the HTHFS.

$$q''_{HTHFS} = h(T_r - T_{S_{HTHFS}}) - q''_{Radiation} \quad (14)$$

The radiation term was included to account for any net radiation leaving the sensor face. Since the HTHFS is painted using Krylon™ ultra flat-black spray paint, the emissivity was assumed to be 0.97 [13]. For all tests, the radiative flux was less than 2% of the convective flux.

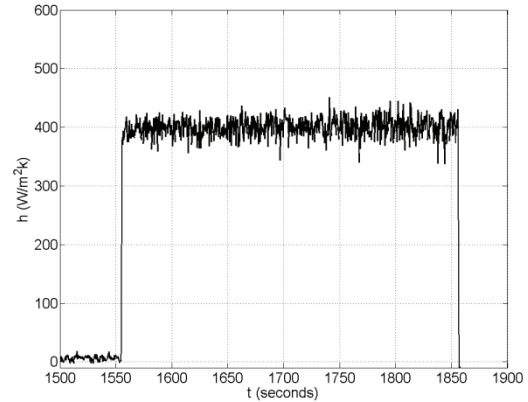


**Fig. 9 Convective heat transfer coefficient**

The calculated heat flux is shown with the output of the HTHFS in Fig. 10 through Fig. 13. Fig. 10 shows the response of the sensor operated as a differential sensor, a slug calorimeter, and using the HHF method while mounted on a water cooled backing. The limitations of the slug calorimeter and differential sensor are obvious. Since the backing is water cooled, this represents the best case scenario for a differential sensor. Although the differential method performs well at steady-state, it has a slow time response. The slug calorimeter does not give an accurate measurement and as the sensor reaches steady-state, the slug calorimeter's output trends to zero. This is as expected and demonstrates why slug calorimeters cannot be used on conductive materials or to measure steady-state heat fluxes.

The HHF method eliminates these problems and performs just as predicted numerically. The HHF has the fast time response of the slug calorimeter, then

trends to the steady-state heat flux more quickly than the differential sensor. This is the exact behavior predicted of the HHF in Fig. 5.

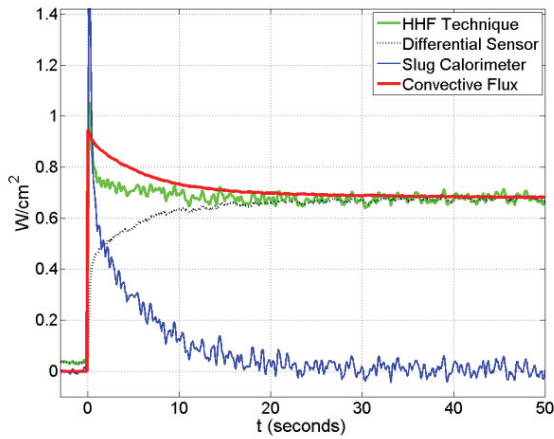


**Fig. 10 Sensor on water cooled backing**

Fig. 11 shows the same test as Fig. 10 except the slug calorimeter's response was calculated using only  $T_2$  and the HHF<sub>2</sub> method was applied. As expected, the overshoot at the beginning of the test is eliminated for the HHF<sub>2</sub> method at the expense of a slower response time. As predicted in Fig. 6, an accurate measurement of the steady-state heat flux is still made.

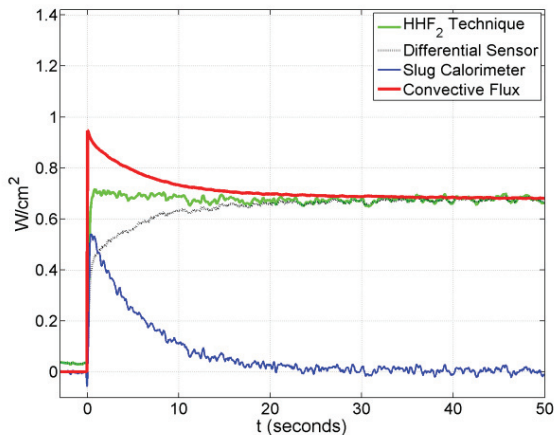


**Fig. 11 Sensor on water cooled backing using only  $T_2$  in slug and hybrid method**

Fig. 12 and Fig. 13 show the response of the sensor mounted on a block of low conductivity, fibrous alumina insulation. Here the curves appear much different than for the water cooled case. In this test, the influx of heat quickly trends to zero. This is because the HTHFS surface temperature quickly warms to the recovery temperature since very little heat leaves the

sensor. That is, the temperature difference driving the heat flow trends to zero causing the heat flux to trend to zero. Although the test time is short, the advantages of the HHF method are still easily recognized. This time, the differential sensor is unable to accurately measure the heat flux. This is because  $q_2''$  is much less than  $q_1''$  which implies that the average of  $q_2''$  and  $q_1''$  is not an accurate measure of  $q_1''$ . On the other hand, since  $q_2''$  is small, the slug calorimeter works relatively well in this case. From Eq. (10), the more  $q_2''$  is minimized (the better the insulation), the more accurately the slug calorimeter will measure  $q_1''$ . As stated previously, in the limit as the backing material becomes a perfect insulator, the HHF method and the slug calorimeter will give identical results once quasi-steady state is reached. Therefore, for any real insulator with non-zero thermal conductivity, the HHF method will outperform the slug calorimeter. This is shown in Fig. 12. Even on this very low conductivity substance, there is still enough heat leaving the back surface of the sensor that the HHF method more accurately measures the heat flux compared to the slug calorimeter.

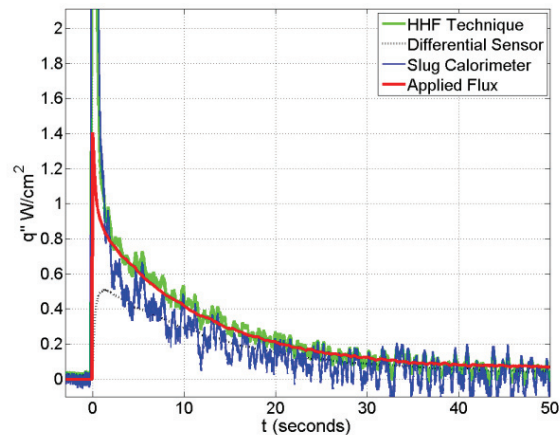


**Fig. 12 Sensor on insulated backing**

Fig. 13 shows the same test as Fig. 12 except only  $T_2$  is used in the slug and hybrid analysis. Once again, the HHF<sub>2</sub> method accurately measures the heat flux with a much smaller overshoot. Here it is more difficult to see any slower time response. This is reasonable because, as shown in Fig. 6, as the backing material thermal conductivity is reduced, the time response of the HHF<sub>2</sub> improves. More experimentation is needed to fully examine the time response characteristics of sensors utilizing the various forms of the hybrid method. Finally, it is worth noting that the HHF<sub>2</sub> outputs in Fig. 11 and Fig. 13 show less noise than their HHF counterparts in Fig. 10 and Fig. 12. This is due to the fact that any fluctuations in surface temperature (due to turbulence in the jet in this case) have been

significantly dampened by the time they reach the back of the sensor. Conversely, the noise would be even worse if only the surface temperature ( $T_1$ ) were used as in Fig. 7.

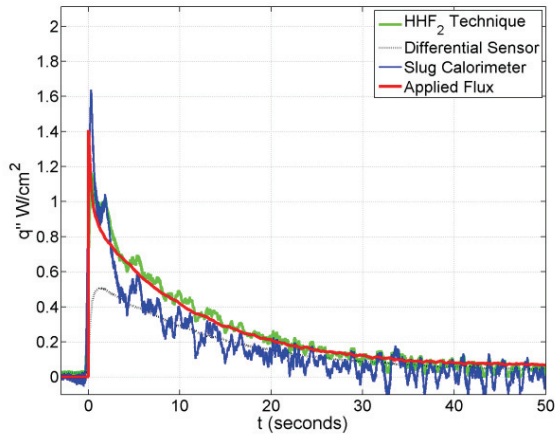


**Fig. 13 Sensor on insulated backing using only  $T_2$  in slug and hybrid method**

It is worth reiterating that a water-cooled backing is the best case scenario for a differential sensor just as an insulated backing is the best case scenario for a slug calorimeter. These represent the two extremes. The hybrid heat flux method performs as well as both the slug calorimeter and the differential sensor at the two extremes and outperforms them anywhere in between.

## 6. Conclusions

This paper outlines a hybrid method for obtaining surface heat flux measurements. It is shown that by combining both spatial and temporal temperature measurements in a hybrid method, the time response and accuracy of heat flux sensors can be improved. More importantly, the hybrid method causes the response to be much less dependent on the properties of the material to which the sensor is mounted. All that is required of the sensor for this method to be applied is for the histories of the top and bottom surface temperatures as well as the temperature drop across the sensor to be measured. In addition, it was shown that by adjusting how the temperatures used in the HHF method were weighted, the hybrid method could be specifically tailored to a particular test. The hybrid method was validated by performing numerical simulations which were supported by experimentation. These results show significant improvements compared to operating the sensor as solely a spatial or temporal heat flux sensor.

## Acknowledgments

The authors would like to acknowledge the support of NASA Dryden Flight Research Center through Tao

of Systems Integration Inc. and contract monitor Larry Hudson. Also the support of the Virginia Space Grant Consortium is gratefully acknowledged.

## Nomenclature

$C$	=	specific heat
$\Delta t$	=	time between temperature measurements, inverse of sampling frequency
$Fo$	=	Fourier number, $ta/\delta^2$
$k$	=	thermal conductivity
$q''$	=	heat flux
$q_0''$	=	step change heat flux for simulation
$q_1''$	=	heat flux into sensor face
$q_2''$	=	heat flux out of sensor back
$\rho$	=	density
$t$	=	time
$t_{ss}$	=	time to reach steady-state
$T_1$	=	temperature at sensor face
$T_2$	=	temperature at sensor back
$T_{ave}$	=	average sensor temperature
$\alpha$	=	thermal diffusivity of sensor, $k/\rho C$
$\delta$	=	thickness of sensor

## References

1. Diller, T.E., *Advances in Heat Flux Measurement*, in *Advances in Heat Transfer*. 1993, Academic Press: Boston. p. 279-368.
2. Hager, N.E.J., *Thin Foil Heat Meter*. Review of Scientific Instruments, 1965. **36**: p. 1564-1570.
3. Hightower, T.M., R.A. Olivares, and D. Philippidis, *Thermal Capacitance (Slug) Calorimeter Theory Including Heat Losses and Other Decaying Processes*. NASA, 2008. **TM-200-0215364**.
4. Kidd, C.T. and J.C. Adams, *Fast-response heat-flux sensor for measurement commonality in hypersonic wind tunnels*. Journal of Spacecraft and Rockets, 2001. **38**(5): p. 719-729.
5. Epstein, A.H., et al., *High-Frequency Response Heat-Flux Gauge*. Review of Scientific Instruments, 1986. **57**(4): p. 639-649.
6. Liebert, C.H., *High Temperature Plug-Type Heat Flux Gauges*. NASA, 1992. **TM 105403**.
7. Rooke, S., G. Fralick, and C. Liebert, *Heat transfer analysis of a plug-type heat flux gauge*. Journal of Thermophysics and Heat Transfer, 1998. **12**(4): p. 536-542.
8. Oishi, T., et al., *Thermal Sensor Development and Testing for NASA Entry Probe Thermal Protection Systems*, in *AIAA Aerospace Sciences Meeting and Exhibit*. 2006: Reno, NV.
9. Gifford, A.R., et al., *A Durable Heat Flux Sensor for Extreme Temperature and Heat Flux Environments*. submitted to AIAA Journal of Thermophysics and Heat Transfer, 2009.

10. Incropera, F. and D. DeWitt, *Introduction to Heat Transfer, 5th ed.*, ed. J.W. Sons. 2002, New York.
11. Gifford, A.R., A. Hoffie, and T.E. Diller, *Convection Calibration of Schmidt-Boelter Heat Flux Gages in Shear and Stagnation Air Flow*. submitted to AIAA Journal of Thermophysics and Heat Transfer, 2009.
12. Holmberg, D.G. and T.E. Diller, *High-frequency heat flux sensor calibration and modeling*. Journal of Fluids Engineering-Transactions of the Asme, 1995. **117**(4): p. 659-664.
13. Kidd, C., *Determination of the Uncertainty of Experimental Heat-Flux Calibrations*, in *AEDC Report TR-83-13*. 1983.